The elementary unit of store-operated Ca^{2+} entry: local activation of CRAC channels by STIM1 at ER–plasma membrane junctions

Riina M. Luik, Minnie M. Wu, JoAnn Buchanan, and Richard S. Lewis

Department of Molecular and Cellular Physiology, Stanford University School of Medicine, Stanford, CA 94305

The activation of store-operated Ca^{2+} entry by Ca^{2+} store depletion has long been hypothesized to occur via local interactions of the endoplasmic reticulum (ER) and plasma membrane, but the structure involved has never been identified. Store depletion causes the ER Ca^{2+} sensor stromal interacting molecule 1 (STIM1) to form puncta by accumulating in junctional ER located 10–25 nm from the plasma membrane (see Wu et al. on p. 803 of this issue). We have combined total internal reflection fluorescence (TIRF) microscopy and patch-clamp recording to localize STIM1 and sites of Ca^{2+} influx through open Ca^{2+} release–activated Ca^{2+} (CRAC) channels in Jurkat T cells after store depletion. CRAC channels open only in the immediate vicinity of STIM1 puncta, restricting Ca^{2+} entry to discrete sites comprising a small fraction of the cell surface. Orai1, an essential component of the CRAC channel, colocalizes with STIM1 after store depletion, providing a physical basis for the local activation of Ca^{2+} influx. These studies reveal for the first time that STIM1 and Orai1 move in a coordinated fashion to form closely apposed clusters in the ER and plasma membranes, thereby creating the elementary unit of store-operated Ca^{2+} entry.

Introduction

A wide variety of cell-surface receptors produce Ca^{2+} signals resulting from the release of Ca^{2+} from intracellular stores followed by Ca^{2+} entry through channels in the plasma membrane. This Ca^{2+} entry process, termed capacitative or store-operated Ca^{2+} entry (SOCE), is evoked by the depletion of Ca^{2+} from the lumen of the ER and drives several critical cellular functions, including growth, motility, secretion, and gene expression (Parekh and Putney, 2005). The best-studied store-operated channel (SOC) is the highly Ca^{2+}-selective Ca^{2+} release–activated Ca^{2+} (CRAC) channel found in lymphocytes and other hematopoietic cells, which is absolutely required for T cell activation by antigen (Feske et al., 2001; Lewis, 2001).

The structural and mechanistic basis of SOCE has remained a mystery since its first proposal, by Putney (1986). The central issue is how the depletion of Ca^{2+} from the lumen of the ER controls the activation of SOCs in the plasma membrane. From the outset, it was assumed that the ER was physically in close apposition to the plasma membrane in order for it to communicate with channels in the plasma membrane. This assumption was based primarily on observations that, in some cells, store refilling was absolutely dependent on extracellular Ca^{2+} ($Ca^{2+}{}_o$) and could occur without a detectable rise in intracellular free Ca^{2+} concentration ($[Ca^{2+}]_i$). These results implied an intimate relationship between ER and plasma membrane, in effect creating a private pathway for store refilling. Although the initial concept of direct coupling between the ER and plasma membrane was later abandoned, indirect evidence continued to support the idea that the ER is close to Ca^{2+} entry sites in the plasma membrane (Putney, 1990). Consistent with this view, in oocytes and astrocytes, fluorescence signals from store-operated Ca^{2+} influx were highest in regions having the highest density of ER (Jaconi et al., 1997; Golovina, 2005). There has been much speculation that the connection between the ER and plasma membrane may resemble the dyad and triad junctions underlying excitation–contraction coupling in muscle. In these cells, the sarcoplasmic reticulum (SR) is positioned within 10–20 nm of the T-tubule (plasma membrane) to enable Ca^{2+} channels in the plasma membrane to trigger the release of Ca^{2+} from

Correspondence to Richard S. Lewis: rslewis@stanford.edu

Abbreviations used in this paper: 2-APB, 2-aminoethyldiphenyl borate; $Ca^{2+}{}_o$, extracellular Ca^{2+}; $[Ca^{2+}]_i$, intracellular free Ca^{2+} concentration; CRAC, Ca^{2+} release–activated Ca^{2+}; IRM, interference reflection microscopy; SOC, store-operated channel; SOCE, store-operated Ca^{2+} entry; SR, sarcoplasmic reticulum; STIM1, stromal interacting molecule 1; TG, thapsigargin; TIRF, total internal reflection fluorescence.

The online version of this article contains supplemental material.

© The Rockefeller University Press $8.00
The Journal of Cell Biology, Vol. 174, No. 6, September 11, 2006 815–825
http://www.jcb.org/cgi/doi/10.1083/jcb.200604015

nearby ryanodine receptors in the SR; in this way, the dyad/triad forms the elementary structural unit of Ca^{2+} release that triggers muscle contraction (Franzini-Armstrong et al., 1999). By analogy, the ER and closely apposed plasma membrane could be considered the elementary unit of SOCE, but the predicted structures, consisting of ER closely coupled to sites of Ca^{2+} influx, have never been identified.

The recent identification of stromal interacting molecule 1 (STIM1) as the probable Ca^{2+} sensor for SOCE offers new strategies in the search for the elementary unit of SOCE. STIM1, a type I ER membrane protein, has a predicted EF-hand domain facing the ER lumen, and mutation of conserved residues likely to be involved in Ca^{2+} binding activates Ca^{2+} influx in cells with full stores (Liou et al., 2005; Zhang et al., 2005). Store depletion causes STIM1 to redistribute from a diffuse localization throughout the ER into puncta near the plasma membrane. This redistribution is likely to be involved in CRAC channel activation, because the constitutively active EF-hand mutants of STIM1 show this distribution even when stores are full (Liou et al., 2005; Zhang et al., 2005). Moreover, puncta formation slightly precedes the opening of CRAC channels, consistent with a causal role in SOC activation (see Wu et al. on p. 803 of this issue). Interestingly, ultrastructural analysis shows that puncta correspond to the accumulation of STIM1 in discrete regions of junctional ER lying within 10–25 nm of the plasma membrane (Wu et al., 2006). The proximity of STIM1 puncta to the plasma membrane is close enough to permit local interactions with proteins in the plasma membrane, including Orai1, which has recently been identified as an essential part of the CRAC channel (Feske et al., 2006; Vig et al., 2006; Zhang et al., 2006).

These new studies raise important questions about how STIM1 transmits the activation signal to CRAC channels in the plasma membrane. Do junctional ER structures containing STIM1 provide the proximal stimulus for the activation of CRAC channels by store depletion? Are CRAC channels activated only locally at sites of STIM1 accumulation or more generally throughout the surrounding plasma membrane? What constitutes the basic unit of SOCE? To answer these questions and better understand how Ca^{2+} store content regulates CRAC channel activity, the spatial relationship between STIM1, Orai1, and open CRAC channels must be determined.

In this study, we have combined total internal reflection fluorescence (TIRF) microscopy and patch-clamp recording to determine the location of active CRAC channels relative to that of STIM1 in the ER. We find that CRAC channel activation in store-depleted cells is tightly restricted to regions directly apposed to STIM1 puncta. These results show for the first time that Ca^{2+} influx through CRAC channels is not widely dispersed throughout the cell but, rather, is highly concentrated in areas juxtaposed to junctional ER that comprise only a small fraction of the cell surface. Store depletion also causes Orai1 to accumulate at these sites, providing a physical basis for the local activation of CRAC channels by STIM1. These results identify the elementary unit of SOCE and show that it is a dynamic assembly, arising from the coordinated migration of the Ca^{2+} sensor and its target channel to closely apposed sites in the ER and the plasma membrane.

Results

Mapping the spatial distribution of open CRAC channels using TIRF microscopy

The location and density of open CRAC channels was determined by measuring local steady-state $[Ca^{2+}]_i$ gradients at the plasma membrane after depleting Ca^{2+} stores. For this purpose, we adapted a method that had been used previously to localize Ca^{2+} entry through ryanodine receptors in cardiac myocytes (Song et al., 1998) and voltage-gated Ca^{2+} channels in excitable cells (Zenisek et al., 2003). Jurkat T cells were dialyzed through the whole-cell recording pipette with 200 μM fluo-5F, a low-affinity, fast-binding Ca^{2+} indicator, together with an excess (10 mM) of the higher affinity, slower binding Ca^{2+} chelator, EGTA. EGTA binds Ca^{2+} too slowly to significantly diminish Ca^{2+} binding to fluo-5F close to channels, but the higher affinity and concentration of EGTA enables it to outcompete fluo-5F for Ca^{2+} binding at distances >1 μm from the source (Zenisek et al., 2003), thus restricting the fluo-5F signals to the vicinity of open channels. Further restriction of the signals in the z dimension is afforded by TIRF microscopy, which restricts excitation to distances within ∼200 nm of the membrane.

Our protocol for localizing Ca^{2+} influx sites is described in Fig. 1. Intracellular Ca^{2+} stores were depleted by intracellular dialysis with EGTA to ensure maximal CRAC channel activation. Voltage clamp was used to control the driving force for Ca^{2+} entry and, thus, the flux through open channels. At +38 mV, the driving force is minimal, and control images at this potential show dim baseline fluorescence (Fig. 1 B, F_1 and F_2). Hyperpolarization to −122 mV elicits a rapid fluorescence increase as Ca^{2+} enters the cell, and depolarization back to +38 mV rapidly terminates the signal. The baseline fluorescence of cells was generally nonuniform, presumably because of spatial variations in dye concentration and illumination. Therefore, to isolate the Ca^{2+}-dependent signal, the fluorescence change in each image ($\Delta F = F - F_0$, where F_0 is the mean of control images F_1 and F_2) was divided by F_0. Typically, the Ca^{2+}-dependent fluorescence signal, $\Delta F/F_0$, develops fully within 10–60 ms of hyperpolarization and dissipates equally quickly upon depolarization (Fig. 1, B and C), leaving behind a small, slowly decaying signal that reflects a small increase in global $[Ca^{2+}]_i$ (see the following section).

Given that Ca^{2+} influx through CRAC channels has never been visualized before at a microscopic scale, it is important to confirm that these signals do in fact reflect CRAC channel activity. Currents recorded during these experiments show the inward rectification and dependence on $Ca^{2+}{}_o$ that are typical of I_{CRAC} (Fig. 1 D). Further evidence that the signals are due to CRAC channels comes from pharmacological experiments. The currents and the fluorescence signals evoked by hyperpolarization were both inhibited by La^{3+} and 2-aminoethyldiphenyl borate (2-APB), known blockers of CRAC channels (Hoth and Penner, 1993; Prakriya and Lewis, 2001; Fig. 2, A and B). Finally, fluorescence changes were minimal in Jurkat CJ-1 cells (Fig. 2 C), a mutant line defective in CRAC channel activity (Fanger et al., 1995). In all cases, the $\Delta F/F_0$ signal was strongly correlated with the level of I_{CRAC} measured electrophysiologically, confirming

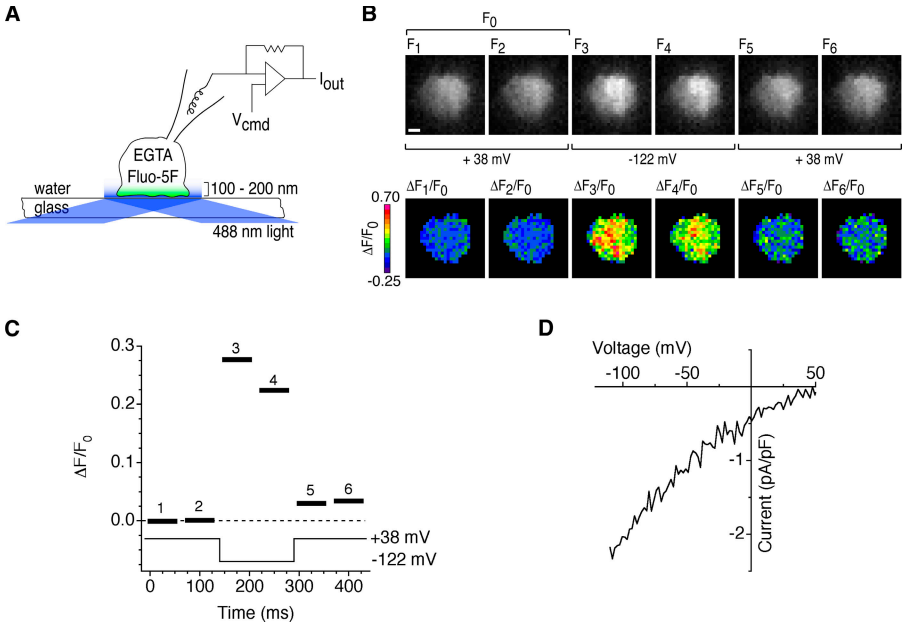

Figure 1. **A method for visualizing active CRAC channels.** (A) TIRF imaging during whole-cell recording from a single Jurkat cell. EGTA and fluo-5F are introduced into the cell through the recording pipette. TIRF illumination restricts the excitation of fluo-5F to within ~200 nm of the coverslip, and EGTA suppresses increases in global $[Ca^{2+}]_i$ while it depletes Ca^{2+} stores. The patch-clamp command voltage (V_{cmd}) controls the driving force for Ca^{2+} entry through open CRAC channels. (B) Fluo-5F fluorescence images show a rapid, reversible fluorescence increase during a voltage step from +38 to −122 mV. $\Delta F/F_0$ images (bottom) were calculated by normalizing raw fluorescence images (top) to the mean of two control images collected at +38 mV (F_0). Bar, 2 µm. (C) $\Delta F/F_0$ values averaged over the cell footprint (black bars) for each ratiometric image. $\Delta F/F_0$ values change within 10–60 ms of changes in membrane potential. The bar width indicates the camera exposure time. (D) Current evoked by voltage ramps from −122 to +50 mV during the experiment, showing the inward rectification typical of I_{CRAC}.

that the fluo-5F fluorescence signals result from Ca^{2+} entry through CRAC channels.

Fluo-5F fluorescence monitors local Ca^{2+} influx near CRAC channels

Several observations provide evidence that fluo-5F monitors predominantly local Ca^{2+} signals near CRAC channels. First, the rapid rise in $\Delta F/F_0$ after membrane hyperpolarization is consistent with the rapid generation of a steady-state $[Ca^{2+}]_i$ elevation near open channels, whereas the rapid dissipation of the signal upon depolarization is expected from the kinetics of diffusion out of this microdomain (Klingauf and Neher, 1997). The rapid dissipation of the signal upon depolarization was incomplete; a small residual fraction of the signal (typically <10% of the peak) decayed back to baseline over tens of seconds. This time course is similar to the rate of Ca^{2+} clearance from Jurkat T cells by the plasma membrane Ca^{2+}-ATPase operating near resting $[Ca^{2+}]_i$ (Bautista et al., 2002), suggesting that the residual signal is due to a small rise in global cell $[Ca^{2+}]_i$. Consistent with this interpretation, the residual signal was relatively uniform across the cell, whereas the rapidly changing (local) signal was heterogenous (Figs. 1 B and 3 B).

A second, more stringent test of the $\Delta F/F_0$ signal as a local detector of open CRAC channels is to compare the time course of fluorescence and I_{CRAC} as CRAC channels undergo Ca^{2+}-dependent inactivation. Because of the speed of Ca^{2+} diffusion

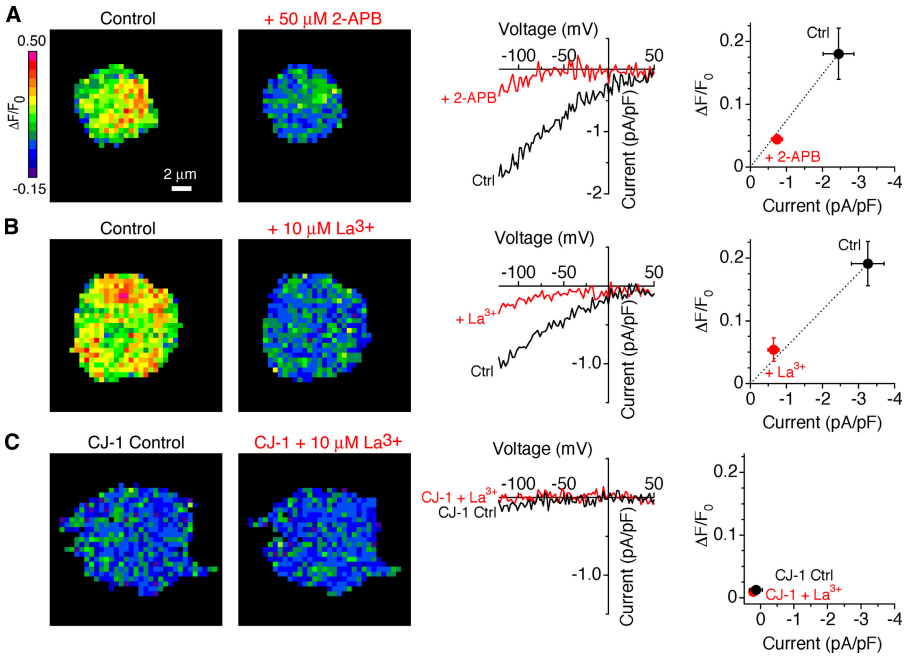

Figure 2. **Fluo-5F fluorescence signals arise from CRAC channels.** Pseudocolor images indicate $\Delta F/F_0$ at –122 mV from three cells as described in Fig. 1 A. $\Delta F/F_0$ signals (left) and membrane currents (middle) are inhibited by 2-APB (A) and La^{3+} (B). (C) $\Delta F/F_0$ signals are absent in CRAC-deficient CJ-1 Jurkat cells. The slight suppression of fluorescence by 10 µM La^{3+} is consistent with the residual amount of I_{CRAC} observed in CJ-1 cells. The graphs on the right show that the $\Delta F/F_0$ signals vary in proportion to I_{CRAC} for all conditions. A, $n = 6$ cells; B, $n = 4$ cells; C, $n = 4$ cells.

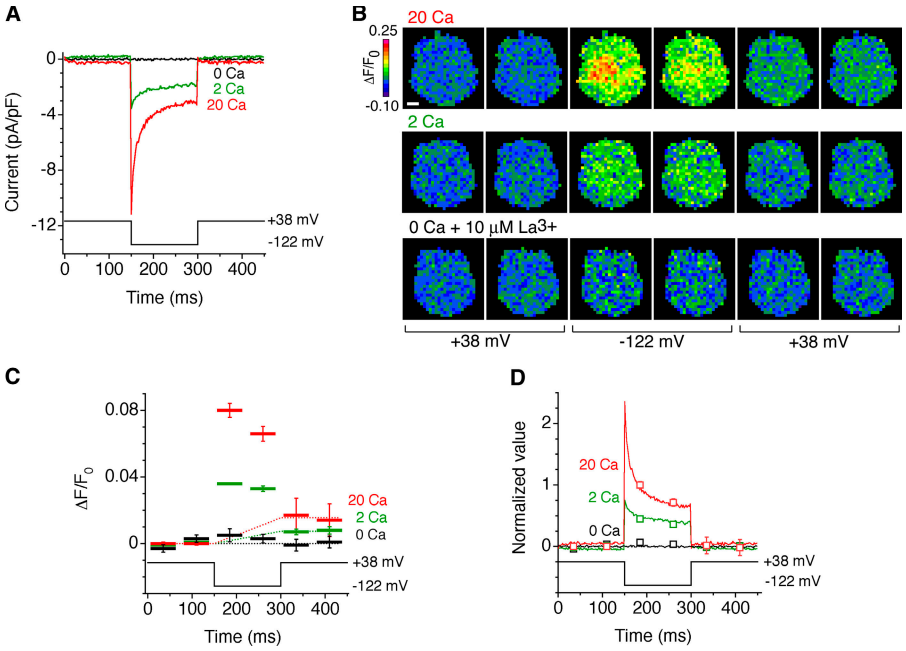

Figure 3. **Fluo-5F monitors local $[Ca^{2+}]_i$ near open channels.** (A) Fast Ca^{2+}-dependent inactivation of I_{CRAC}. Current responses of a single cell to hyperpolarization in the presence of 0, 2, or 20 mM Ca^{2+} are shown. (B) $\Delta F/F_0$ images acquired during the current recordings shown in A. Bar, 2 μm. (C) $\Delta F/F_0$ plotted with voltage for each of the images in B, averaged over four stimulus presentations. The dashed lines show the estimated rise of the global component of $\Delta F/F_0$ for each $[Ca^{2+}]_o$. (D) The $\Delta F/F_0$ signal closely tracks the time course of I_{CRAC}, indicating that it monitors local $[Ca^{2+}]_i$ near CRAC channels. $\Delta F/F_0$ values (squares) after subtraction of the global component are plotted relative to the maximal $\Delta F/F_0$ image (acquired from 10–60 ms after a hyperpolarizing voltage step in 20 mM Ca^{2+}_o). I_{CRAC} traces (solid lines) are normalized to the mean I_{CRAC} during acquisition of the maximal $\Delta F/F_0$ image.

into the cell, local $[Ca^{2+}]_i$ close to channels is expected to vary in proportion to the current amplitude, whereas the global $[Ca^{2+}]_i$ should more closely follow the time integral of the current. In response to hyperpolarization, CRAC channels undergo rapid inactivation because of a local effect of incoming Ca^{2+} (Hoth and Penner, 1993; Zweifach and Lewis, 1995). The size of the current and the speed and extent of inactivation increase as $[Ca^{2+}]_o$ is increased from 2 to 20 mM (Fig. 3 A). Simultaneous fluorescence measurements also indicate a rapid decline in $\Delta F/F_0$ during the 150-ms hyperpolarization, which is enhanced by increasing $[Ca^{2+}]_o$ (Fig. 3, B and C). To compare the time course and amplitude of the current with those of $\Delta F/F_0$, we first corrected $\Delta F/F_0$ for the buildup of global $[Ca^{2+}]_i$, assuming for simplicity that the global $\Delta F/F_0$ component increases linearly during the hyperpolarization. The corrected values of $\Delta F/F_0$ are plotted together with the absolute value of the current in Fig. 3 D, with both datasets normalized to a value of 1 at the time of the first image collected at –122 mV in 20 mM Ca^{2+}_o. The $\Delta F/F_0$ signal closely tracks both the time-dependent decline in I_{CRAC} because of inactivation as well as the reduced amplitude of I_{CRAC} at lower $[Ca^{2+}]_o$. These results provide strong confirmation that the rapidly developing component of $\Delta F/F_0$ is a valid indicator of local $[Ca^{2+}]_i$ near open CRAC channels.

The ability to resolve Ca^{2+} influx sites is limited by the diffusional spread of Ca^{2+} bound fluo-5F molecules. This can be measured empirically from the spatial $\Delta F/F_0$ profile produced by a point source of Ca^{2+} influx. Serendipitously, we found that exposure of cells to unattenuated 488-nm laser illumination for >40 s evoked a light-activated increase in a nonselective leak conductance, which was associated with "hotspots" of fluo-5F fluorescence (Fig. 4, A–C). During maintained high-intensity illumination, these hotspots fluctuated, blinking on and off at various locations. These events appeared to be unrelated to CRAC channels, as they were insensitive to 100 μM 2-APB

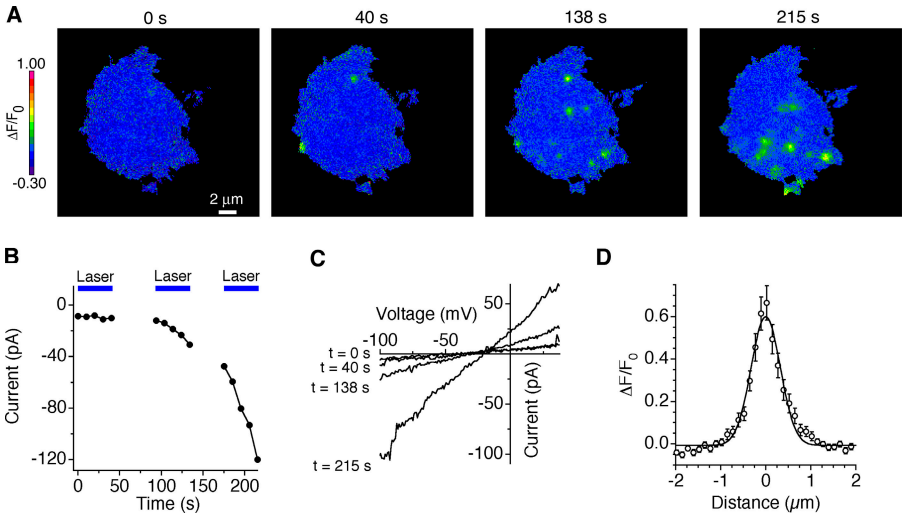

Figure 4. **Ca^{2+} influx through a light-activated pathway can be localized with submicrometer resolution.** (A) Induction of light-activated Ca^{2+} influx in CRAC-deficient CJ-1 Jurkat mutants during repeated exposures to unattenuated 488-nm laser light. After 40 s of constant illumination, discrete sites of Ca^{2+} influx began to appear at the cell footprint; the magnitude and prevalence of these Ca^{2+} "hotspots" increased with prolonged laser illumination. Voltage, −112 mV. (B) Mean inward current at −112 mV during the experiment in A. Blue bars indicate periods of laser illumination. (C) Current–voltage relations collected during the same experiment show induction of a nonselective conductance. (D) The mean radial spread of $\Delta F/F_0$ through cross-sections of 32 hotspots. A Gaussian curve fitted to the data shows that $\Delta F/F_0$ declines by 50% within 377 nm.

and 10 μM La^{3+} and arose with similar frequency in control and CRAC-deficient CJ-1 Jurkat cells (unpublished data). The dimensions of the hotspots were relatively uniform, suggesting that they represent influx sites smaller than the overall spatial resolution of our Ca^{2+}-detection system and therefore approximate a point source. The mean intensity profile of the hotspots followed a Gaussian function that decayed by 50% within 377 nm and by 90% within 644 nm (Fig. 4 D). This is significantly broader than the resolution of the microscope optics (the Airy disc decays by 50% within 86 nm), indicating that the measured $\Delta F/F_0$ profile is mostly determined by diffusion of Ca^{2+} and fluo-5F. The spatial spread of the $\Delta F/F_0$ signal agrees reasonably well with that predicted by a simple reaction-diffusion model for a point source of Ca^{2+} flowing into 200 μM fluo-5F and 10 mM EGTA (50% decay within 490 nm; see Materials and methods). Together with the results of Figs. 2 and 3, these data demonstrate that the $\Delta F/F_0$ signal can be used to map the location of active CRAC channels in the cell footprint with submicrometer resolution.

CRAC channels open in close proximity to STIM1 puncta

The spatial relationship between STIM1 puncta and active CRAC channels was determined by simultaneously visualizing STIM1 and Ca^{2+} influx sites in individual cells. For separation of fluorescently labeled STIM1 and fluo-5F fluorescence, we labeled STIM1 with a monomeric red fluorescent protein (Cherry-STIM1; Shaner et al., 2004). Jurkat cells transfected with Cherry-STIM1 were loaded with fluo-5F and imaged by TIRF microscopy; during the period between break-in and the start of recording, Cherry-STIM1 accumulated in puncta (Fig. 5 D). Upon hyperpolarization to −122 mV, transfected cells exhibited robust Ca^{2+} influx through CRAC channels (Fig. 5, A and B); to minimize contributions from global $[Ca^{2+}]_i$, fluorescence data were collected only at short times (10–60 ms) after hyperpolarization. The distributions of both Ca^{2+} influx density and Cherry-STIM1 puncta were nonuniform, with the highest densities of each near the center of the cell footprint (Fig. 5, A and D). To facilitate comparisons of the two maps, contour lines of Ca^{2+} influx density in pseudocolor are overlaid on the image of Cherry-STIM1 fluorescence in Fig. 5 E. The spatial distributions of Ca^{2+} influx and Cherry-STIM1 overlap but are not identical. Peaks of influx are not always centered on Cherry-STIM1 puncta, and some Cherry-STIM1 puncta are not associated with peaks of Ca^{2+} influx (Fig. 5 E). Similar results were obtained in eight other cells. Unfortunately, the close spacing of the puncta complicates interpretation of these images; if clusters of active channels are separated by less than the spatial resolution of the $[Ca^{2+}]_i$ measurement (~400 nm), superposition of their Gaussian fluorescence profiles will generate a maximum signal between the clusters. Because most of the Cherry-STIM1 puncta are separated by <400 nm, individual Ca^{2+} influx sites cannot be unequivocally assigned to specific puncta.

To clarify more precisely the relationship between STIM1 and active CRAC channels, we sought conditions that would increase the separation of STIM1 puncta. We tried several approaches that were unsuccessful; for example, partial depletion of stores with cyclopiazonic acid reduced the intensity of puncta but not their number. Depolymerization of microtubules with nocodazole caused the ER to coalesce into a clump near the center of the footprint and caused cells to detach from the coverslip (unpublished data). However, the actin depolymerizing agent cytochalasin D, added together with or after thapsigargin (TG), dramatically increased the space between STIM1 puncta. 5 μM cytochalasin D caused Cherry-STIM1 puncta to coalesce into larger structures within several min (Fig. 6 A and Video 1, available at http://www.jcb.org/cgi/content/full/jcb.200604015/DC1) without affecting footprint adherence as monitored by interference reflection microscopy (IRM; Fig. 6 B). A similar fusion of ER tubules into larger structures was noted in cells expressing ER-targeted fluorescent proteins after exposure to either 5 μM cytochalasin D or 20 μM latrunculin A (unpublished data).

Several independent lines of evidence indicate that cytochalasin D treatment after store depletion preserves the normal

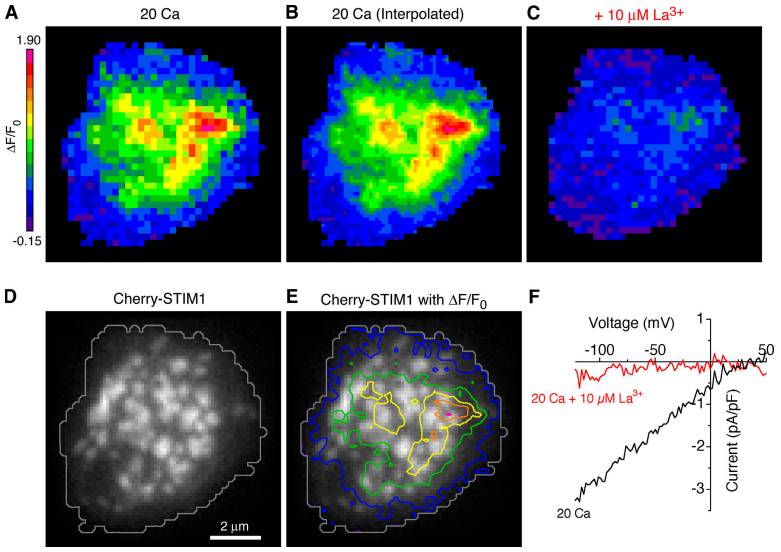

Figure 5. **Regions of CRAC-mediated Ca^{2+} influx overlap with STIM1 puncta.** (A) $\Delta F/F_0$ image from a Jurkat cell collected 10–60 ms after a hyperpolarizing voltage step to −122 mV. (B) Linear interpolation of the $\Delta F/F_0$ image in A to equalize the number of pixels to the Cherry-STIM1 image in D. (C and F) 10 μM La^{3+} inhibited both $\Delta F/F_0$ and I_{CRAC} in this cell, confirming that $\Delta F/F_0$ arises from CRAC channels. (D) TIRF image of Cherry-STIM1 in the same cell. A gray contour line outlines the fluo-5F footprint depicted in A. (E) Pseudocolored contour lines of Ca^{2+} influx density from B overlaid on the Cherry-STIM1 image show the overlap of Ca^{2+} influx sites with Cherry-STIM1 puncta.

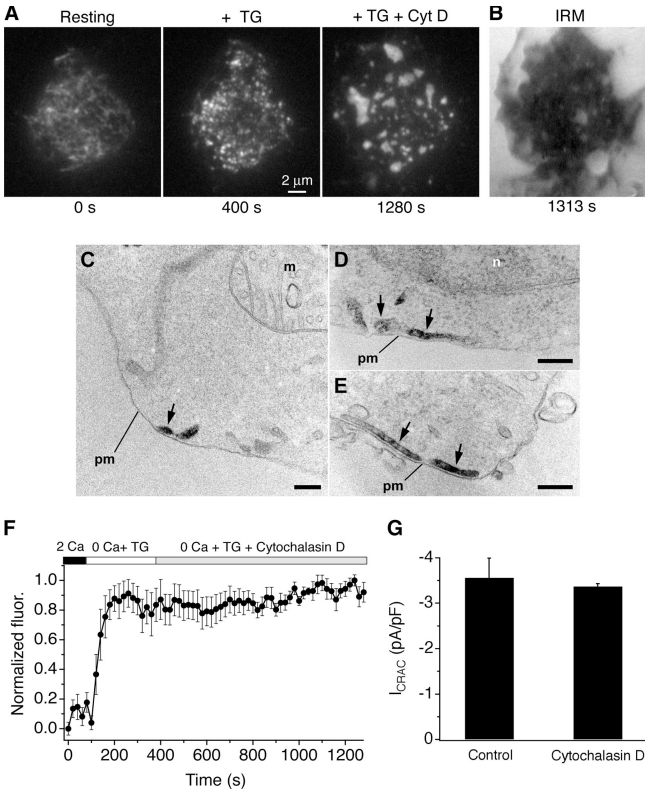

Figure 6. **Cytochalasin D reorganizes STIM1 puncta in Jurkat cells.** (A) TIRF images of Cherry-STIM1 in an intact cell. Initially, Cherry-STIM1 was diffusely distributed within the ER (left) but redistributed into puncta after 5 min of treatment with 0 mM $Ca^{2+}{}_o$ plus 1 mM EGTA and 1 μM TG (middle). After a subsequent 15-min exposure to 5 μM cytochalasin D, the puncta coalesced into large, sparsely distributed structures (right). The complete image sequence is shown in Video 1 (available at http://www.jcb.org/cgi/content/full/jcb.200604015/DC1). (B) An IRM image of the cell footprint after 16 min of cytochalasin D treatment shows persistent adherence of the cell to the coverslip. (C–E) Electron micrographs from cells treated with TG plus cytochalasin D as in A, showing the distribution of HRP-STIM1 in ER tubules (arrows) located next to the plasma membrane (pm). n, nucleus; m, mitochondrion. Bars, 200 nm. (F) Cytochalasin D does not affect the integrated fluorescence of Cherry-STIM1 puncta near the plasma membrane. The fluorescence increases in response to store depletion (TG) because of the formation of puncta but is constant after 15 min of subsequent cytochalasin D treatment ($n = 7$ cells). (G) Cytochalasin D does not affect maintenance of I_{CRAC}. I_{CRAC} density was measured at −122 mV in Cherry-STIM1–transfected cells after >15 min of pretreatment with TG ± 5 μM cytochalasin D ($n = 4$ cells each). Because I_{CRAC} activates well before cytochalasin D causes any noticeable changes in ER structure, this experiment tests its effect on the maintenance rather than the activation of I_{CRAC}.

CRAC channel activation mechanism in Jurkat cells. First, cytochalasin D did not disrupt the close association of STIM1 puncta with the plasma membrane, as determined at the ultrastructural level using Jurkat cells expressing the HRP-STIM1 fusion protein. Cytochalasin D treatment after store depletion caused HRP-STIM1 to accumulate in ER tubules in close proximity to the plasma membrane (Fig. 6, C–E), similar to what was seen in the absence of the drug (Wu et al., 2006). Second, cytochalasin D did not affect the total near-membrane Cherry-STIM1 fluorescence (Fig. 6 F), suggesting that the drug reorganizes existing STIM1 puncta without altering the amount of STIM1 near the plasma membrane. Finally, I_{CRAC} density was also unaffected by cytochalasin D (Fig. 6 G), showing at a functional level that the drug and the ensuing reorganization of STIM1 puncta leaves the CRAC channel activation mechanism intact.

By reducing the number of puncta, cytochalasin D pretreatment allowed better resolution of the spatial relationship between Cherry-STIM1 and Ca^{2+} influx sites (Fig. 7, A and B). In seven cells treated in this way, Ca^{2+} influx sites were all tightly associated with STIM1 puncta, although, as in control cells (Fig. 5), not all puncta were associated with influx (Fig. 7, C and D; and Fig. S1, available at http://www.jcb.org/cgi/content/full/jcb.200604015/DC1). The spatial profiles of the Ca^{2+} signal and STIM1 fluorescence were compared for 23 individual influx sites from seven cells, with one example shown in Fig. 7 E. Typically, the width of the $\Delta F/F_0$ signal was greater than expected from a single point source (Fig. 4), suggesting that each influx site represents a cluster of open CRAC channels. The spatial profile of the Ca^{2+} signal was similar to but consistently wider than that of the associated STIM1 punctum. To estimate how much of this difference might be attributable to diffusion of Ca^{2+} and fluo-5F from CRAC channels, we convolved the STIM1 distribution with a Gaussian function describing the spread of the fluo-5F signal. The resulting curve overlaps quite closely with the observed $\Delta F/F_0$ distribution, with the widths of the two curves differing by <200 nm (Fig. 7 E). The similarity of the fluo-5F and convolved STIM1 fluorescence profiles indicates that CRAC channels only open in extremely close proximity to STIM1.

In principle, the local activation of CRAC channels could arise if STIM1 produces a local signal, i.e., one that only activates channels in the immediate vicinity; alternatively, the channels themselves may be confined to the vicinity of STIM1 puncta. Orai1 has recently been identified in several studies as an essential component of the CRAC channel (Feske et al., 2006; Vig et al., 2006; Zhang et al., 2006). To visualize the distribution of CRAC channels relative to STIM1, we transfected cells with Cherry-STIM1 and GFP-myc-Orai1. At rest, there is little overlap between Cherry-STIM1 and GFP-myc-Orai1. TIRF imaging shows that Cherry-STIM1 is localized to the ER, whereas GFP-myc-Orai1 is distributed across the cell footprint (Fig. 8 A). Wide-field epifluorescence images taken through the cell center show that Orai1 in resting cells is diffusely distributed at the cell perimeter and in membrane ruffles, suggesting a location in the plasma membrane (Feske et al., 2006), in marked contrast to the ER distribution of STIM1 (Fig. S2 A, available at http://www.jcb.org/cgi/content/full/jcb.200604015/DC1). Remarkably, after store depletion, both Cherry-STIM1 and GFP-myc-Orai1 redistribute into a punctate pattern with a high degree of colocalization (Fig. 8 B, right; and Fig. S2 B). Subsequent treatment with cytochalasin D caused puncta to coalesce, and STIM1 and Orai1 remained colocalized (Fig. 8 C), further supporting our conclusion that cytochalasin D reorganizes the CRAC activation machinery without disrupting it. Most important, the accumulation of Orai1 near STIM1 puncta suggests a physical mechanism for the local activation of CRAC channels and Ca^{2+} influx at these sites. Together, these results reveal the structure and dynamic nature of the elementary unit of SOCE.

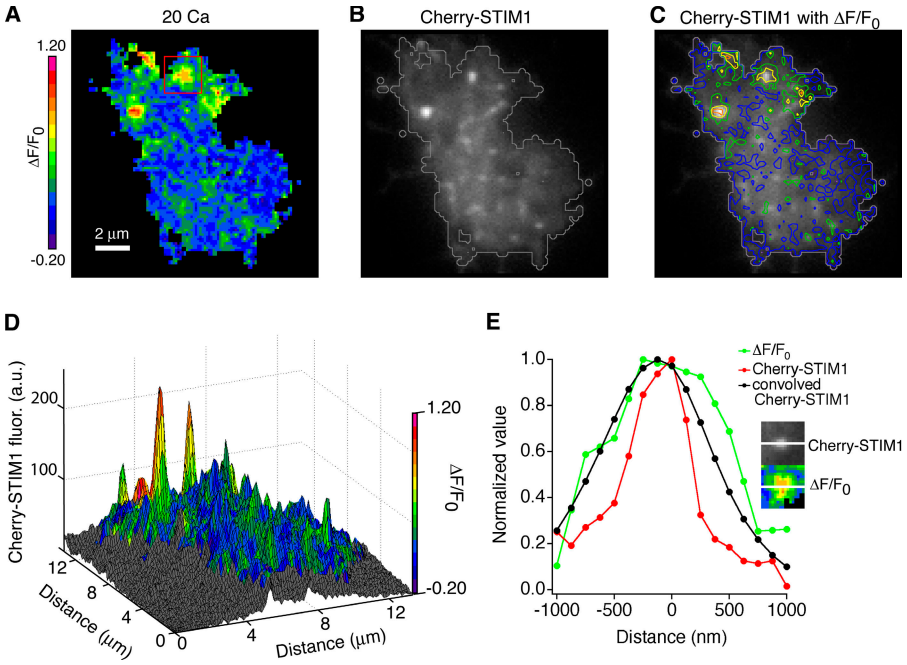

Figure 7. **Open CRAC channels colocalize with STIM1 puncta in cytochalasin D–treated cells.** TIRF images of $\Delta F/F_0$ (A) and Cherry-STIM1 fluorescence (B) in a Jurkat cell treated for 15 min with 0-Ca^{2+} Ringer's plus 1 mM EGTA, 1 μM TG, and 5 μM cytochalasin D. $\Delta F/F_0$ was linearly interpolated as in Fig. 5 B. A gray contour line outlines the fluo-5F footprint in B. (C) Pseudocolored contour lines of Ca^{2+} influx density overlaid on the Cherry-STIM1 image show that Ca^{2+} influx sites are associated with bright STIM1 puncta. (D) Overlay of the pseudocolored $\Delta F/F_0$ map on a surface plot of Cherry-STIM1 fluorescence. (E) Comparison of the spatial extent of Cherry-STIM1 and $\Delta F/F_0$ at a single Ca^{2+} influx site. The intensity profiles through the center of a single Cherry-STIM1 punctum and its associated Ca^{2+} influx site (inset; taken from the boxed area in A) are shown. The radial spread of $\Delta F/F_0$ is centered on the Cherry-STIM1 profile. Convolution of the Cherry-STIM1 fluorescence curve with the diffusional spread function for fluo-5F yields a curve (black line) that is similar in extent to $\Delta F/F_0$.

Discussion

Although the activation of store-operated Ca^{2+} channels by store depletion is well established, the cellular structures and events involved in this process have remained obscure since the first proposal of the capacitative Ca^{2+} entry hypothesis 20 yr ago. We applied a TIRF-based method for Ca^{2+} signal localization to determine for the first time the location of active CRAC channels relative to the ER Ca^{2+} sensor STIM1. Our results show a remarkably close association of open channels with STIM1 puncta that parallels the distribution of Orai1, a component of the CRAC channel, after store depletion. These studies, together with those of Wu et al. (2006), define for the first time the elementary unit of SOCE, consisting of a cluster of STIM1 in the junctional ER membrane locally activating an associated cluster of CRAC channels in the closely apposed plasma membrane.

A method for mapping the locations of active CRAC channels

To measure local Ca^{2+} influx through CRAC channels, we adapted a method originally developed to visualize Ca^{2+} signals from small clusters of active ryanodine receptors and voltage-gated Ca^{2+} channels in excitable cells (Song et al., 1998; Zenisek et al., 2003). Localizing influx through active CRAC channels is particularly challenging because of their exceedingly small unitary conductance, which is estimated to be >100-fold smaller than that of voltage-gated Ca^{2+} channels (Zweifach and Lewis, 1993; Prakriya and Lewis, 2002), as well as the small whole-cell CRAC currents they generate in nonexcitable cells (typically <2 pA/pF). As a consequence, we typically observed a $\Delta F/F_0$ of only 10–20% in Jurkat cells, compared with the three- to fourfold change reported in neurons and hair cells (Zenisek et al., 2003).

The small Ca^{2+} signals from CRAC channels made it imperative to distinguish them from other Ca^{2+} entry pathways using pharmacological blockers and a CRAC-deficient mutant Jurkat cell line (Fig. 2). One example of such a pathway was the nonselective Ca^{2+}-permeable leak conductance that was activated by unattenuated 488-nm light. These influx sites were clearly distinguished from CRAC channels by their insensitivity to 100 μM 2-APB and 10 μM La^{3+} and their presence in I_{CRAC}-deficient Jurkat mutants. They also appear to be distinct from the light-activated Ca^{2+}-permeable channels reported in other cell types (Mendez and Penner, 1998), which are activated most efficiently at near-UV wavelengths (340–380 nm) and are inhibited >50% by 10 μM La^{3+}. However, despite placing constraints on the maximum laser intensity that could be applied, these light-activated hotspots provided a convenient means of determining the spatial resolution of the Ca^{2+} imaging technique (Fig. 4), which had dimensions close to those expected from theory (half-widths of 377 and 490 nm, respectively).

STIM1 activates CRAC channels through a local signaling event

To distinguish between local and global activation of CRAC channels by store depletion, we determined the spatial relationship between STIM1 puncta and open CRAC channels. In Jurkat cells with depleted Ca^{2+} stores, the density of Ca^{2+} influx was highest in the vicinity of STIM1 puncta, but there was generally not a well-defined 1:1 relationship between puncta and peaks of influx density. Unfortunately, the spacing of puncta was close enough that summation of neighboring Ca^{2+} profiles would be predicted to obscure the location of individual Ca^{2+} influx sites.

We used cytochalasin D as a tool to overcome these problems by reducing the number of STIM1 puncta. In Jurkat cells, cytochalasin D caused STIM1 puncta to coalesce into large,

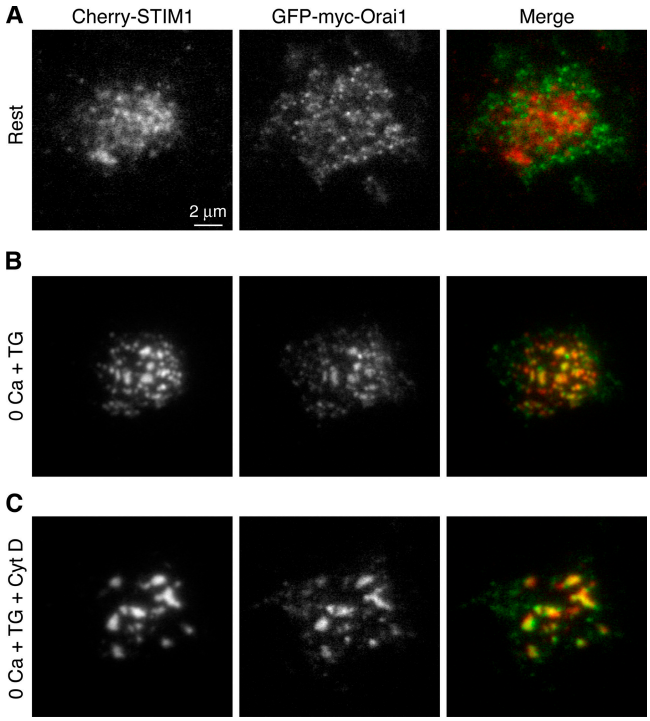

Figure 8. **Orai1 colocalizes with STIM1 at peripheral ER–plasma membrane junctions after store depletion.** TIRF imaging of a Jurkat cell transiently coexpressing Cherry-STIM1 and GFP-myc-Orai1 before and after store depletion. (A) In cells bathed in 2 mM Ca^{2+}, Cherry-STIM1 is distributed throughout the ER (left), whereas GFP-myc-Orai1 is distributed throughout the cell footprint (middle). The merged image (right) shows little overlap of Orai1 (green) and STIM1 (red). (B) After a 5-min treatment with 1 μM TG in 0-Ca^{2+} Ringer's plus 1 mM EGTA, both Cherry-STIM1 (left) and GFP-myc-Orai1 (middle) colocalize at discrete puncta, as shown in the merged image (right). Similar results were seen in 14 out of 16 cells. (C) After a subsequent 15-min exposure to 5 μM cytochalasin D, Cherry-STIM1 (left) and GFP-myc-Orai1 (middle) remained localized in coalesced puncta (right).

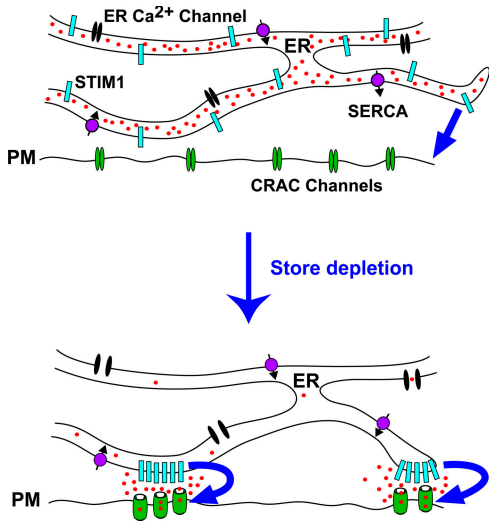

Figure 9. **Local activation of CRAC channels by STIM1 at ER–plasma membrane junctions.** Store depletion causes STIM1 to accumulate in preexisting and newly formed regions of junctional ER, whereas Orai1 accumulates in apposed regions of the plasma membrane. CRAC channels open only in the close vicinity of the STIM1 puncta. The convergence of STIM1 and Orai1 at ER–plasma membrane junctions creates the elementary unit of SOCE.

sparsely distributed structures, possibly through the fusion of ER tubules (Fig. 6). Similar effects of cytochalasin D on ER structure have been reported in other cells, but the mechanism is not well understood (Al-Mohanna et al., 1997; Ribeiro et al., 1997). For this reason, it was important to verify that cytochalasin D did not alter the activation mechanism of the CRAC channel in any significant way. Four lines of evidence indicate that cytochalasin D merely reorganizes the CRAC activation components without changing their structural or functional properties (Figs. 6 and 8). The total STIM1 fluorescence measured by TIRF remains constant, indicating that the amount of STIM1 near the membrane is unchanged. Electron microscopy measurements show that junctional ER containing high levels of STIM1 remains intact. Orai1 remains associated with STIM1 puncta during and after cytochalasin D treatment, directly demonstrating that the trigger (STIM1) and the effector (Orai1) of SOCE maintain their spatial relationship relative to each other. Finally, I_{CRAC} itself remains constant during treatment with cytochalasin D, demonstrating at a functional level that the coupling between store depletion and channel activation is preserved. Together, these experiments confirm that the relationship between STIM1 and CRAC channels in Jurkat cells is conserved both structurally and functionally in the presence of cytochalasin D.

It should be noted, however, that the effects on cytochalasin D may be cell specific. As in Jurkat cells, cytochalasin D does not affect the maintenance of SOCE or I_{CRAC} in rat basophilic leukemia, smooth muscle, and corneal epithelial cells, but it has an inhibitory effect in platelets and pancreatic acinar cells (Rosado et al., 2005). An explanation for these differences will require further study but may reflect a varying ability of cytochalasin D to disrupt the coupling between the peripheral ER and the plasma membrane.

In store-depleted cells treated with cytochalasin D, areas of Ca^{2+} influx were tightly associated with STIM1 puncta (Fig. 7 and Fig. S1). After taking into account the spread of Ca^{2+} and fluo-5F by diffusion, the overlap between the STIM1 fluorescence and the Ca^{2+} influx signal is close enough to suggest that STIM1 only activates CRAC channels located in its immediate vicinity. Although all sites of high Ca^{2+} influx were associated with a STIM1 punctum, a minority of puncta were not paired with a peak of Ca^{2+} influx. One possibility is that some puncta are not close to a sufficiently high number of CRAC channels to generate detectable Ca^{2+} influx. Overall, these results show that Ca^{2+} influx through CRAC channels is not widely dispersed throughout the cell but, rather, is concentrated in specialized subregions that make up a small fraction of the cell surface.

The presence of discrete Ca^{2+} influx sites provides an effective mechanism for enhancing the specificity of store-operated Ca^{2+} signals. Ca^{2+}-sensitive adenylate cyclases are known to be activated exclusively or preferentially by SOCE over other influx pathways (Fagan et al., 1996). Similarly, there is evidence that local $[Ca^{2+}]_i$ elevation near CRAC channels is a potent modulator of plasma membrane Ca^{2+}-ATPase activity in T cells (Bautista et al., 2002). These studies suggest a close physical coupling of

the CRAC channel to specific downstream targets; given the low conductance of the CRAC channel, colocalization with a cluster of CRAC channels at a junctional complex would expose targets to a potent but highly local activation signal, enhancing specificity. It will be interesting in future studies to determine whether these and other Ca^{2+}-dependent proteins are localized to the ER–plasma membrane junctions containing STIM1 and Orai1.

The elementary unit of SOCE is dynamic

Our results and those of Wu et al. (2006) describe a sequence of early structural and functional steps in the activation of SOCE (Fig. 9). Depletion of Ca^{2+} stores initiates a series of events, beginning with the redistribution of STIM1 located throughout the ER to its accumulation in regions of junctional ER lying within 10–25 nm of the plasma membrane. New regions of junctional ER also form, and Orai1 accumulates at sites in the plasma membrane directly opposite STIM1. Shortly after the arrival of STIM1 at junctional sites, CRAC channels begin to open in the apposed plasma membrane.

The local activation of CRAC channels in the plasma membrane by STIM1 in the junctional ER defines the elementary unit of SOCE. These contacts are reminiscent of the structurally well-defined dyad and triad junctions between the SR and T-tubule membrane that underlie excitation–contraction coupling in skeletal and cardiac muscle (Cheng et al., 1993; Franzini-Armstrong et al., 1999). In both cases, a protein in one membrane (voltage-gated Ca^{2+} channel or STIM1) triggers the opening of Ca^{2+} channels in the opposite membrane (ryanodine receptor or CRAC, respectively), and in both cases the membranes are separated by a gap of only ~10–20 nm. In muscle cells, activation signals are passed across the gap by either a diffusible messenger (Ca^{2+} in cardiac myocytes) or conformational coupling between Ca^{2+} channels and ryanodine receptors (in skeletal muscle). Likewise, CRAC channels could be activated by a diffusible messenger or by direct contact with STIM1, perhaps through coiled-coil interactions of STIM1 and Orai1. However, a fundamental difference between these two systems is that the muscle dyad is a static structure, whereas the SOC junction is labile. Neither STIM1 nor Orai1 reside permanently at junctional sites, unlike the voltage-gated Ca^{2+} channel and ryanodine receptor of muscle. Rather, the stimulus itself, store depletion, directs the assembly of the SOCE unit in a dynamic manner by triggering the redistribution of STIM1 and Orai1 and inducing their colocalization at junctional sites. This study reveals a novel mode of channel activation, in which both the sensor and the target channel itself must migrate to a common site to interact. The mechanism by which the coordinated translocation of these proteins in two membrane-delimited compartments occurs has yet to be determined.

Materials and methods

Cell lines and reagents

Jurkat E6-1 cells (American Type Culture Collection) and the CJ-1 mutant Jurkat cell line (Fanger et al., 1995) were maintained as described previously (Bautista et al., 2002). 2-APB and cytochalasin D were obtained from Sigma-Aldrich, TG was purchased from LC Laboratories, and fluo-5F was obtained from Invitrogen.

Plasmids

Cherry-STIM1 plasmid was constructed by inserting mCherry (a gift from R. Tsien, University of California, San Diego, La Jolla, CA) after the signal sequence of human STIM1 (Origene). mCherry was amplified by PCR from mCherry-pRSET-B (Shaner et al., 2004) with primers 5′-ttattaggtaccatggtgagcaagggc-3′ and 5′-ataataggtacccttgtacagctcgtccat-3′ to append KpnI sites onto each end. After KpnI digestion, mCherry was ligated into a unique engineered KpnI site in STIM1 (Quickchange XL kit; Stratagene) at 1188–1193 bp. The HRP-STIM1 plasmid was constructed as described by Wu et al. (2006). N-terminally myc-tagged WT Orai1 (a gift from S. Feske, Harvard Medical School, Boston, MA) in the Gateway entry vector pENTR11 (Feske et al., 2006) was inserted into the Gateway destination vector pDS_GFP-XB by recombination reaction using enzyme mix (Gateway LR Clonase; Invitrogen) to generate GFP-myc-Orai1. For transient transfection, 10^7 cells were electroporated (Gene Pulser; Bio-Rad Laboratories) with 10 μg plasmid DNA 48–72 h before imaging.

TIRF microscopy

Cells were allowed to adhere to poly-L-lysine–coated coverslip chambers and were bathed in extracellular solution containing 155 mM NaCl, 4.5 mM KCl, 2 or 20 mM $CaCl_2$, 1 mM $MgCl_2$, 10 mM D-glucose, and 5 mM Na-Hepes, pH 7.4. 0-Ca^{2+} Ringer's solution was nominally Ca^{2+} free except in cytochalasin D experiments, when 2 mM $MgCl_2$ plus 1 mM EGTA was added. Illumination at 488 and 514.5 nm was supplied by a 100-mW argon-ion laser (Enterprise 622; Coherent, Inc.) coupled via a single-mode fiber (Point Source) and a TILL-TIRF condenser (Till Photonics) to a microscope (Axiovert 200M; Carl Zeiss MicroImaging, Inc.) equipped with a 100× α-Plan Fluar objective (NA 1.45; Carl Zeiss MicroImaging, Inc.). For 488-nm excitation (fluo-5F and GFP), the filter cube contained a 1.0 neutral density in series with a Z488/10 excitation filter, a Q505LP dichroic mirror, and a HQ535/50M emission filter (all filters were obtained from Chroma Technology Corp.). A 510 LP emission filter was used when imaging fluo-5F in untransfected cells. For 514.5-nm excitation (Cherry-STIM1), the filter cube contained a 0.5 neutral density in series with a HQ535/45 excitation filter, a Q570LP dichroic mirror, and an E610LPV2 emission filter. Neutral densities were omitted when imaging GFP-myc-Orai1 and Cherry-STIM1. Images were acquired with a cooled charge-coupled device camera (ORCA-ER; Hamamatsu). Cherry-STIM1 images were captured with 250–500-ms camera exposures at 2 × 2 camera pixel binning. In GFP-myc-Orai1 and Cherry-STIM1 colocalization experiments, images were captured at 1 × 1 pixel binning 3–4 s apart to allow time for filter cube switching. All imaging functions were controlled by MetaMorph software (Molecular Devices). All experiments were performed at room temperature (22–25°C).

IRM and electron microscopy

Cells were imaged with epi-illumination at 460 nm using a Polychrome II monochromator (Till Photonics); a 455DCLP allowed collection of 460-nm light reflected at both the glass–solution and solution–cell interfaces. If the distance between these interfaces is <230 nm, an interference pattern is generated where destructive interference is maximal at the smallest separation between the cell and the coverslip (Verschueren, 1985). Electron microscopy was performed as described by Wu et al. (2006).

Patch-clamp electrophysiology

Patch-clamp experiments were conducted in the standard whole-cell recording configuration as previously described (Zweifach and Lewis, 1995). The standard internal solution contained 140 mM Cs aspartate, 3 mM $MgCl_2$, 10 mM EGTA, 10 mM Hepes, and 0.2 mM fluo-5F, pH 7.3 with CsOH. In Cherry-STIM1 experiments, fluo-5F concentration was reduced to 0.1 mM to minimize contamination of the Cherry fluorescence signal. Currents were filtered at 1 kHz and sampled at 2 kHz without series resistance compensation. Voltage stimuli consisted of a 100-ms step to −122 mV followed by a 100-ms ramp from −122 to +50mV. Unless indicated, all data were leak subtracted using currents collected in nominally Ca^{2+}-free bath solution plus 10 μM $LaCl_3$. Three to four sweeps were averaged for each displayed current.

Combined imaging and patch-clamp recording

Simultaneous imaging and patch-clamp measurements were performed using in-house software developed on the Igor Pro platform interfaced with an input/output board (ADAC 1300; Molecular Devices) that simultaneously controlled the charge-coupled device camera, the laser shutter, and the amplifier (Axopatch 200B; Molecular Devices). The voltage was alternated between +38 and −122 mV every 150 ms to generate five hyperpolarizing

steps. 50-ms camera exposures were collected 10 and 85 ms after each voltage step. Camera pixels were binned to 8 × 8 when imaging fluo-5F in untransfected cells or to 4 × 4 in cells transfected with Cherry-STIM1.

Data analysis

Image analysis was performed using NIH ImageJ software. All raw fluorescence images were dark-noise subtracted and thresholded to three to four times the remaining background. For fluo-5F experiments, the F_0 image was generated by averaging two images collected at +38 mV. F_0 was subtracted from each image, and the result was divided by F_0 to yield $\Delta F/F_0$. Unless indicated, each displayed $\Delta F/F_0$ image is a mean derived from four voltage stimulus presentations.

Contour plots were generated using Igor Pro, and pseudocolored surface plots were generated using MatLab (Mathworks). Means are expressed ± SEM. Figures were prepared using Photoshop and Illustrator (Adobe).

Estimating the spatial resolution of $\Delta F/F_0$

The predicted radial spread of Ca^{2+}–fluo-5F from a point source was calculated for 0.2 mM fluo-5F and 10 mM EGTA (Zenisek et al., 2003). As Ca^{2+} enters the cell, the fraction of Ca^{2+} bound to fluo-5F (R) depends on the binding rate constants for fluo-5F ($k_{on,fluo\text{-}5F} = 2.36 \times 10^8\ M^{-1}s^{-1}$) and EGTA ($k_{on,EGTA} = 2.5 \times 10^6\ M^{-1}s^{-1}$):

$$R = k_{on,fluo\text{-}5F}[fluo\text{-}5F] / \left(k_{on,fluo\text{-}5F}[fluo\text{-}5F] + k_{on,EGTA}[EGTA]\right)$$

Initially, upon Ca^{2+} entry, 65% of Ca^{2+} is bound to fluo-5F. The spread of Ca^{2+}–fluo-5F is determined by the unbinding rate constant for fluo-5F ($k_{off,fluo\text{-}5F} = 543\ s^{-1}$) and its diffusion coefficient ($D_{fluo\text{-}5F} = 40\ \mu m^2/s$). On average, fluo-5F will diffuse 379 nm before unbinding Ca^{2+}, and 65% of this released Ca^{2+} will again be bound by fluo-5F. This reaction–diffusion cycle results in a 50% decay of the Ca^{2+}–fluo-5F signal within 490 nm.

The radial spread of Ca^{2+}–fluo-5F was directly measured from Ca^{2+} influx hotspots in CJ-1 cells evoked by constant unattenuated 488-nm laser light. 50-ms images were acquired every 150 ms at 2 × 2 pixel binning; two control images were collected at +18 mV, and nine consecutive images were collected at −112 mV. This stimulus was repeated at 10-s intervals until hotspots of light-activated Ca^{2+} influx were detected.

Online supplemental material

Fig. S1 shows that active CRAC channels colocalize with STIM1 after cytochalasin D treatment. Fig. S2 shows that STIM1 and Orai1 colocalize after store depletion. Video 1 shows that cytochalasin D reorganizes STIM1 puncta in Jurkat cells. Online supplemental material is available at http://www.jcb.org/cgi/content/full/jcb.200604015/DC1.

The authors thank the members of the Lewis Laboratory for helpful discussions during the course of this work, Thomas Karpati for help with MatLab, and Miriam Goodman and Pam Pappone for comments on the manuscript. We would also like to thank Roger Tsien for the gift of mCherry, Stephan Feske for the gift of myc-Orai1, and Franklin Mullins and Chan Young Park for generating the GFP-myc-Orai1 construct.

This work was supported by Stanford Graduate Fellowship and National Institutes of Health training grant GM007276 (to R.M. Luik), National Institutes of Health National Research Service Award postdoctoral training grant 5T32A107290-21 (to M.M. Wu), National Institutes of Health grant GM45374 (to R.S. Lewis), and a gift from the Mathers Charitable Foundation (to R.S. Lewis).

Submitted: 5 April 2006
Accepted: 14 August 2006

References

Al-Mohanna, F.A., E.J. Pettit, and M.B. Hallett. 1997. Does actin polymerization status modulate Ca^{2+} storage in human neutrophils? Release and coalescence of Ca^{2+} stores by cytochalasins. *Exp. Cell Res.* 234:379–387.

Bautista, D.M., M. Hoth, and R.S. Lewis. 2002. Enhancement of calcium signalling dynamics and stability by delayed modulation of the plasma-membrane calcium-ATPase in human T cells. *J. Physiol.* 541:877–894.

Cheng, H., W.J. Lederer, and M.B. Cannell. 1993. Calcium sparks: elementary events underlying excitation-contraction coupling in heart muscle. *Science.* 262:740–744.

Fagan, K.A., R. Mahey, and D.M. Cooper. 1996. Functional co-localization of transfected Ca^{2+}-stimulable adenylyl cyclases with capacitative Ca^{2+} entry sites. *J. Biol. Chem.* 271:12438–12444.

Fanger, C.M., M. Hoth, G.R. Crabtree, and R.S. Lewis. 1995. Characterization of T cell mutants with defects in capacitative calcium entry: genetic evidence for the physiological roles of CRAC channels. *J. Cell Biol.* 131:655–667.

Feske, S., J. Giltnane, R. Dolmetsch, L.M. Staudt, and A. Rao. 2001. Gene regulation mediated by calcium signals in T lymphocytes. *Nat. Immunol.* 2:316–324.

Feske, S., Y. Gwack, M. Prakriya, S. Srikanth, S.H. Puppel, B. Tanasa, P.G. Hogan, R.S. Lewis, M. Daly, and A. Rao. 2006. A mutation in Orai1 causes immune deficiency by abrogating CRAC channel function. *Nature.* 441:179–185.

Franzini-Armstrong, C., F. Protasi, and V. Ramesh. 1999. Shape, size, and distribution of Ca^{2+} release units and couplons in skeletal and cardiac muscles. *Biophys. J.* 77:1528–1539.

Golovina, V.A. 2005. Visualization of localized store-operated calcium entry in mouse astrocytes. Close proximity to the endoplasmic reticulum. *J. Physiol.* 564:737–749.

Hoth, M., and R. Penner. 1993. Calcium release-activated calcium current in rat mast cells. *J. Physiol.* 465:359–386.

Jaconi, M., J. Pyle, R. Bortolon, J. Ou, and D. Clapham. 1997. Calcium release and influx colocalize to the endoplasmic reticulum. *Curr. Biol.* 7:599–602.

Klingauf, J., and E. Neher. 1997. Modeling buffered Ca^{2+} diffusion near the membrane: implications for secretion in neuroendocrine cells. *Biophys. J.* 72:674–690.

Lewis, R.S. 2001. Calcium signaling mechanisms in T lymphocytes. *Annu. Rev. Immunol.* 19:497–521.

Liou, J., M.L. Kim, W.D. Heo, J.T. Jones, J.W. Myers, J.E. Ferrell Jr., and T. Meyer. 2005. STIM is a Ca^{2+} sensor essential for Ca^{2+}-store-depletion-triggered Ca^{2+} influx. *Curr. Biol.* 15:1235–1241.

Mendez, F., and R. Penner. 1998. Near-visible ultraviolet light induces a novel ubiquitous calcium-permeable cation current in mammalian cell lines. *J. Physiol.* 507:365–377.

Parekh, A.B., and J.W. Putney Jr. 2005. Store-operated calcium channels. *Physiol. Rev.* 85:757–810.

Prakriya, M., and R.S. Lewis. 2001. Potentiation and inhibition of Ca^{2+} release-activated Ca^{2+} channels by 2-aminoethyldiphenyl borate (2-APB) occurs independently of IP_3 receptors. *J. Physiol.* 536:3–19.

Prakriya, M., and R.S. Lewis. 2002. Separation and characterization of currents through store-operated CRAC channels and Mg^{2+}-inhibited cation (MIC) channels. *J. Gen. Physiol.* 119:487–508.

Putney, J.W., Jr. 1986. A model for receptor-regulated calcium entry. *Cell Calcium.* 7:1–12.

Putney, J.W., Jr. 1990. Capacitative calcium entry revisited. *Cell Calcium.* 11:611–624.

Ribeiro, C.M., J. Reece, and J.W. Putney Jr. 1997. Role of the cytoskeleton in calcium signaling in NIH 3T3 cells. An intact cytoskeleton is required for agonist-induced $[Ca^{2+}]_i$ signaling, but not for capacitative calcium entry. *J. Biol. Chem.* 272:26555–26561.

Rosado, J.A., P.C. Redondo, S.O. Sage, J.A. Pariente, and G.M. Salido. 2005. Store-operated Ca^{2+} entry: vesicle fusion or reversible trafficking and de novo conformational coupling? *J. Cell. Physiol.* 205:262–269.

Shaner, N.C., R.E. Campbell, P.A. Steinbach, B.N. Giepmans, A.E. Palmer, and R.Y. Tsien. 2004. Improved monomeric red, orange and yellow fluorescent proteins derived from *Discosoma* sp. red fluorescent protein. *Nat. Biotechnol.* 22:1567–1572.

Song, L.S., J.S. Sham, M.D. Stern, E.G. Lakatta, and H. Cheng. 1998. Direct measurement of SR release flux by tracking 'Ca^{2+} spikes' in rat cardiac myocytes. *J. Physiol.* 512:677–691.

Verschueren, H. 1985. Interference reflection microscopy in cell biology: methodology and applications. *J. Cell Sci.* 75:279–301.

Vig, M., C. Peinelt, A. Beck, D.L. Koomoa, D. Rabah, M. Koblan-Huberson, S. Kraft, H. Turner, A. Fleig, R. Penner, and J.P. Kinet. 2006. CRACM1 is a plasma membrane protein essential for store-operated Ca^{2+} entry. *Science.* 312:1220–1223.

Wu, M.M., J. Buchanan, R.M. Luik, and R.S. Lewis. 2006. Ca^{2+} store depletion causes STIM1 to accumulate in ER regions closely associated with the plasma membrane. *J. Cell Biol.* 174:803–813.

Zenisek, D., V. Davila, L. Wan, and W. Almers. 2003. Imaging calcium entry sites and ribbon structures in two presynaptic cells. *J. Neurosci.* 23:2538–2548.

Zhang, S.L., Y. Yu, J. Roos, J.A. Kozak, T.J. Deerinck, M.H. Ellisman, K.A. Stauderman, and M.D. Cahalan. 2005. STIM1 is a Ca^{2+} sensor that

activates CRAC channels and migrates from the Ca^{2+} store to the plasma membrane. *Nature.* 437:902–905.

Zhang, S.L., A.V. Yeromin, X.H. Zhang, Y. Yu, O. Safrina, A. Penna, J. Roos, K.A. Stauderman, and M.D. Cahalan. 2006. Genome-wide RNAi screen of Ca^{2+} influx identifies genes that regulate Ca^{2+} release-activated Ca^{2+} channel activity. *Proc. Natl. Acad. Sci. USA.* 103:9357–9362.

Zweifach, A., and R.S. Lewis. 1993. Mitogen-regulated Ca^{2+} current of T lymphocytes is activated by depletion of intracellular Ca^{2+} stores. *Proc. Natl. Acad. Sci. USA.* 90:6295–6299.

Zweifach, A., and R.S. Lewis. 1995. Rapid inactivation of depletion-activated calcium current (I_{CRAC}) due to local calcium feedback. *J. Gen. Physiol.* 105:209–226.